Clim Dyn (2016) 47:2801–2815
DOI 10.1007/s00382-016-2998-6

Interpreting the inter-model spread in regional precipitation projections in the tropics: role of surface evaporation and cloud radiative effects

Boutheina Oueslati[1,2] · Sandrine Bony[1] · Camille Risi[1] · Jean-Louis Dufresne[1]

Received: 16 June 2015 / Accepted: 16 January 2016 / Published online: 3 February 2016

Abstract In this study, we investigate and quantify different contributors to inter-model differences in regional precipitation projections among CMIP5 climate models. Contributors to the spread are very contrasted between land and ocean. While circulation changes dominate the spread over oceans and continental coasts, thermodynamic changes associated with water vapor increase dominate over inland regions. The inter-model spread in the dynamic component is associated with the change in atmospheric radiative cooling with warming, which largely relates to atmospheric cloud radiative effects. Differences in the thermodynamic component result from the differences in the change in surface evaporation that is explained by decreases in surface humidity and limited surface water availability over land. Secondary contributions to the inter-model spread in thermodynamic and dynamic components result respectively from present-day climatology (owing to the Clausius–Clapeyron scaling) and from the shape of the vertical velocity profile associated with changes in surface temperature gradients. Advancing the physical understanding of the cloud-circulation and precipitation-evaporation couplings and improving their representation in climate models may stand the best chance to reduce uncertainty in regional precipitation projections.

Keywords Precipitation projections uncertainties · Evaporation · Cloud radiative effects

✉ Boutheina Oueslati
boutheina.oueslati@u-bourgogne.fr

[1] LMD, UMR 8539, IPSL, CNRS/Université Pierre et Marie Curie, Paris, France

[2] CRC, UMR 6282 Biogéosciences, CNRS/Université de Bourgogne – Franche-Comté, Dijon, France

1 Introduction

Societies are vulnerable to regional precipitation change in response to global warming because they are directly affected by the water resources distribution, availability and variability. Understanding and anticipating the response of tropical precipitation to climate change is thus highly needed to develop adequate adaptation strategies but it also remains a major challenge. Precipitation projections from general circulation models (GCMs) exhibit some robust features at the global and zonal scales, such as a general intensification of the global hydrological cycle (Held and Soden 2006). This response can be understood by considering the energy balance of the atmosphere (Mitchell et al. 1987; Stephens and Ellis 2008; Previdi 2010; O'Gorman et al. 2012). Indeed, the sensitivity of global mean precipitation to global warming is energetically constrained by the change in the net tropospheric radiative cooling. In response to climate warming, the radiative cooling of the atmosphere is enhanced through increased longwave radiation to space associated with higher atmospheric temperatures. The radiative budget is also affected by radiative feedbacks associated with water vapor and clouds. In addition, the radiative forcing of carbon dioxide can directly influence the radiative cooling rate and therefore precipitation through fast adjustments independent on global-mean surface temperature change (Andrews et al. 2010; Bony et al. 2013). In particular, an increase in GHG concentrations tends to reduce the net radiative cooling of the troposphere, resulting in a reduced rainfall rate and a weakened overturning circulation (Bony et al. 2013). The energetic constraint on global mean precipitation imposes that precipitation increases with surface temperature at a much slower rate (about 2–3 % K^{-1}) than water vapour (about

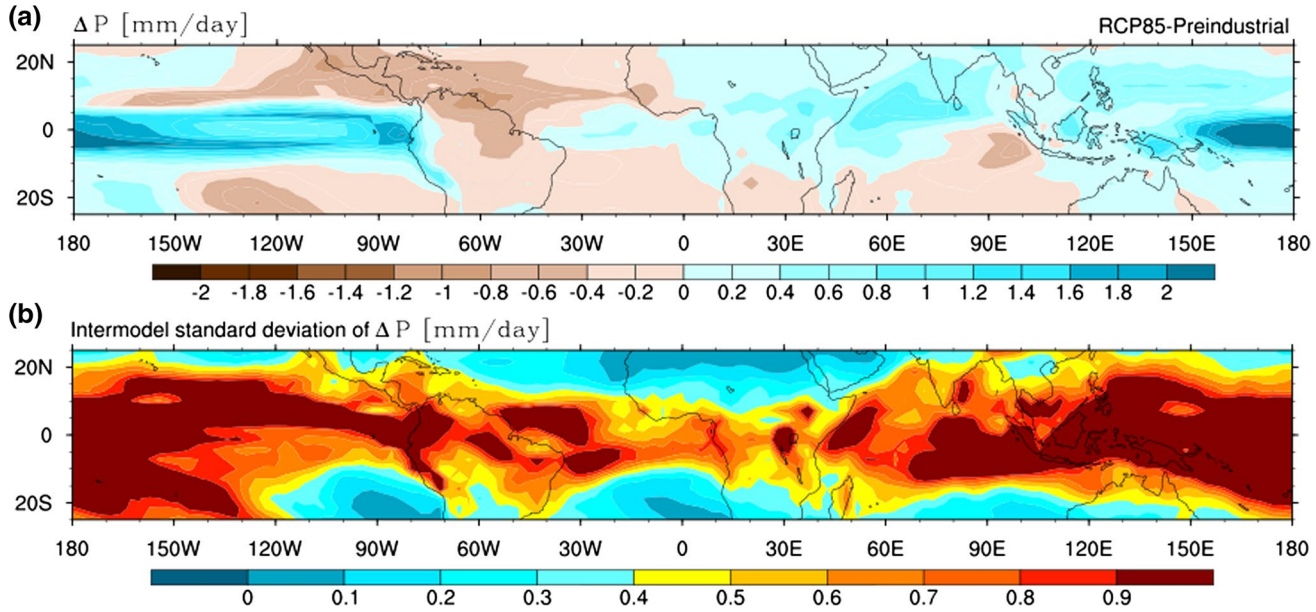

Fig. 1 **a** Projected change in annual precipitation in the tropics for 2081–2100 in the RCP8.5 scenario, relative to 1986–2005 from 15 CMIP5 models summarized in Table 1. **b** Inter-model spread of regional precipitation projections computed as the inter-model standard deviation of precipitation changes

7.5 % K^{-1}) (Mitchell et al. 1987; Held and Soden 2006). This difference implies a slowing down of the tropical circulation (Held and Soden 2006). The weakening of the tropical circulation can be interpreted as a consequence of the change in the dry static stability: Knutson and Manabe (1995) proposed that in subsidence regions radiative cooling increases at a much slower rate than dry static stability in response to global warming. Given that subsidence is constrained by the radiative cooling and the dry static stability, it results in a weakening of downward motions and, owing to mass conservation, in a weakening of the tropical circulation.

Precipitation change at the global scale is explained by robust mechanisms reproduced by all models implying a widespread consensus in hydrological sensitivity across models (Popke et al. 2014, submitted). However, the regional precipitation change exhibits a much lower agreement between models.

The spatial pattern of precipitation change over ocean is characterized, on the large scale, by an increase in precipitation in the wettest regions and a decrease in dry regions (Allen and Ingram 2002; Held and Soden 2006). This is illustrated in Fig. 1a which shows the multi-model annual precipitation projected by CMIP5[1] climate models at the end of the 21st century in RCP8.5 scenario. The wet-get-wetter (WeGW) and dry-get-drier view can be simply understood from the water vapor budget, relating the difference between precipitation and evaporation to the water vapor flux convergence. However, on smaller scales and over land, the WeGW response is less robust because the slowing down of tropical circulation can overwhelm the increase in moisture (Chadwick et al. 2013; Bony et al. 2013; Greve et al. 2014). In addition, the WeGW view does not explain the precipitation pattern in dry regions (e.g. East Africa) and near precipitation margins because of local surface evaporation that partly opposes and sometimes dominates the dry-get-drier response in subsidence regions. Precipitation change is also affected by tropical Sea Surface Temperature (SST) pattern changes, with rainfall increasing in regions where SSTs are warming more than the tropical mean [namely the Warmer get wetter mechanism, Xie et al. (2010)]. This response likely contributes to the large precipitation increase in the equatorial Pacific (see Fig. 1a) where models predict an enhanced equatorial warming (Liu et al. 2005; Xie et al. 2010). These results highlight the importance of both mean and relative SST warming for tropical circulation changes and, in turn, for the resulting precipitation pattern. This was also emphasized by Huang et al. (2013) who showed that both the Warmer get wetter and Wet get wetter mechanisms are important for tropical rainfall change, dominating the annual mean and seasonal anomalies, respectively. However, by comparing Atmospheric General Circulation Model (AGCM) global warming simulations, He et al. (2014) and He and Soden (2015) showed that the warmer

[1] Fifth Phase of the Coupled Models Inter-comparison Project.

get wetter mechanism was relevant mostly over the equatorial oceans, and that elsewhere the regional precipitation response was rather dominated by the direct effect of CO_2 and global warming. In addition to the direct radiative forcing of CO_2 and SST change, land-sea warming contrast may also contribute substantially to the precipitation response (Chadwick et al. 2014; He and Soden 2015).

All these studies contribute to better understand what controls the multi-model mean and robust changes in the precipitation response under global warming. However, precipitation projections still exhibit large disagreements between models at the regional scale. This is shown in Fig. 1b which exhibits the inter-model spread in precipitation among CMIP5 models at the end of the 21st century in RCP8.5 scenario. The largest uncertainties arise over tropical oceans, the Maritime Continent and most of South America. The causes of these uncertainties have not been fully explored. However, some ideas have emerged to explain the inter-model spread in precipitation projections. In particular, because the wet-get-wetter response implies that precipitation changes associated with warming are highly dependent on the present-day pattern of precipitation, biases in the simulation of present-day climatology will lead to biases in the projections of future precipitation change (Mitchell et al. 1987; Bony et al. 2013). In addition, the atmospheric response to changes in global-mean and regional patterns of SST (Stevens and Bony 2013; Ma and Xie 2013) are an important source of inter-model diversity in tropical rainfall projection. Cloud radiative feedbacks and surface sensible heat fluxes are other contributors to the inter-model scatter in the response of precipitation (Previdi 2010). Based on the analysis of idealized simulations from two GCMs, Voigt and Shaw (2015) showed that cloud radiative effects could lead to pronounced changes in the circulation patterns in response to global warming. How much these effects contribute to the spread in regional precipitation projections in a more realistic framework remains an open question.

This paper further examines the mechanisms controlling the regional precipitation response under global warming and the primary sources of inter-model spread. Several questions arise from the different studies documented above: How strong is the dependence of precipitation changes on the present-day pattern of precipitation and associated biases? How much does the uncertainty in climate sensitivity translate into an uncertainty in regional precipitation projection? What processes are contributing to inter-model differences in the large-scale circulation response? How can we explain the contrasted responses between land and ocean in precipitation change that have been highlighted in previous studies (Lambert and Allen 2009; O'Gorman and Muller 2010; Muller and O'Gorman 2011; Greve et al. 2014)?

This paper examines these questions by using the framework of analysis of precipitation and circulation change proposed by Bony et al. (2013). We examine in particular the relative roles of carbon dioxide direct effect and climate warming, as well as dynamical and thermodynamical processes, in the spread of tropical precipitation projections.

The paper is structured as follows. Section 2 describes the data and the methodology used in this study. Section 3 examines the role of dynamic and thermodynamic components, as well as fast and long-term processes in the spread of tropical precipitation projections. Section 4 proposes an interpretation of the inter-model spread and highlights the role of evaporation and cloud radiative effects. These results are summarized in Sect. 5.

2 Data and methodology

2.1 Model data

The analysis is conducted using numerical simulations from 15 state-of-the-art coupled ocean-atmosphere general circulation models (OAGCMs) participating in the Fifth Phase of the Coupled Models Inter-comparison Project [CMIP5, Taylor et al. (2012)] and for which model outputs necessary to our analysis are available. Table 1 summarizes the characteristics of the models used with their names and acronyms and their horizontal and vertical resolutions. We use monthly mean outputs of 30 years of pre-industrial and abrupt $4 \times CO_2$ coupled ocean-atmosphere simulations and 20 years (2080–2099) of representative concentration pathway 8.5 (RCP8.5) simulations.

2.2 Methodology

The change in precipitation is analysed using a framework starting from the monthly-mean vertically-integrated water budget (Bony et al. 2013). Regional precipitation can be decomposed as

$$P = E - [q\nabla \cdot V] - [V \cdot \nabla q], \tag{1}$$

where E is evaporation, $\mathbf{V}$ the horizontal wind, q the vertical profile of specific humidity. Brackets refer to mass-weighted vertical integral. The vertical profile of vertical velocity ω is close to the first baroclinic mode in the tropics. Then, we can decompose it as $\omega = \Omega + (\omega - \Omega)$ where $\Omega(p) = \overline{\omega}\Phi(p)$ with $\overline{\omega}$ is the vertical mean of ω and Φ a specified vertical structure so that $\Omega(p)$ is close to the first baroclinic mode and $\int \Phi(p)\frac{dp}{g} = 1$. More details about the decomposition and the maps of precipitation components can be found in Bony et al. (2013). Then, Eq. 1 can be rewritten as

$$P = E + \overline{\omega}\Gamma_q + V_q + H_q, \tag{2}$$

Table 1 List of models analyzed in this study

Modeling groups	Model name	Atmospheric resolution
National Centre for Atmospheric Research (NCAR)	CCSM4	0.9°x 1.25°-L26
Canadian Centre for Climate Modeling and Analysis	CanESM2	T63-L35
LASG-IAP/LASG, Institute of Atmospheric Physics,Chinese Academy of Sciences (IAP)	FGOALS-s2	2.5°x 4°- L26
Centre National de Recherches Meteorologiques (CNRM)	CNRM-CM5	T127- L31
Atmosphere and Ocean Research Institute (The University of Tokyo), National Institute for Environmental Studies, and Japan Agency for Marine-Earth Scice and Technology (MIROC)	MIROC5 MIROC-ESM	T85-L40 T42-L80
Met Office Hadley Centre (MOHC)	HadGEM2-ES	1.25°× 1.875°- L38
Meteorological Research Institute (MRI)	MRI-CGCM3	TL159-L48
Beijing Climate Center, China Meteorological Administration (BCC)	BCC-CSM1-1	T42-L26
Max Planck Institute for Meteorology (MPI)	MPI-ESM-LR	1.9°x 1.9°- L47
Institute for Numerical Mathematics (INM)	inmcm4	1.5°x 2°- L21
Norwegian Climate Centre (NCC)	NorESM1-M	1.8°x 2.5°- L26
Institut Pierre-Simon Laplace (IPSL)	IPSL-CM5A-LR	1.9°x 3.75°- L39
	IPSL-CM5A-MR	1.25°x 2.5°-L39
	IPSL-CM5B-LR	1.9°x 3.75°-L39

where $\Gamma_q = -[\Phi(p)\frac{\partial q}{\partial p}]$, $V_q = -[(\omega(p) - \Omega(p))\frac{\partial q}{\partial p}]$ corresponding to the deviation of the shape of vertical velocity from the first baroclinic mode and H_q the vertically-integrated horizontal moisture advection ($-[V \cdot \nabla q]$).

The change in monthly-mean precipitation can be expressed as

$$\Delta P = (\Delta E + \Delta H_q + \overline{\omega}\Delta\Gamma_q + \Delta V_q) + \Gamma_q\Delta\overline{\omega} = \Delta P_{ther} + \Delta P_{dyn}, \quad (3)$$

where ΔP_{dyn}, defined as $\Gamma_q\Delta\overline{\omega}$, refers to the dynamic component and is related to large-scale vertical motion changes. It constitutes a leading term in the dynamically-induced changes in precipitation. ΔP_{ther} is referred to as the thermodynamic component because it is strongly impacted by changes in water vapor. Owing to the large contribution of Clausius–Clapeyron relationship to water vapor changes, ΔP_{ther} exhibits a wet-get-wetter and dry-get-drier response associated with increased moisture convergence in the moist ascending regions and moisture divergence in the dry subsiding regions (Bony et al. 2013).

3 Inter-model spread in precipitation projections

3.1 Dynamic and thermodynamic contributions: contrasted responses between land and ocean

To examine the relative roles of the dynamic and thermodynamic components in inter-model differences, we regress each of these two components against the total precipitation change, so that $\Delta P_{ther} = a_{ther}\Delta P + b_{ther}$ for the thermodynamic component and $\Delta P_{dyn} = a_{dyn}\Delta P + b_{dyn}$ for the dynamic component, where $a_{ther,dyn}$ and $b_{ther,dyn}$ are respectively the slope and the intercept of the linear regression. The slopes of the regression quantify the contribution of each component to the total spread. Areas where the correlation of (ΔP_{ther}, ΔP) and (ΔP_{dyn}, ΔP), and thus the linear regression, is not statistically significant at the 95% confidence level are masked. The patterns are shown in Fig. 2.

The dynamic and thermodynamic slopes show contrasted responses between land and ocean. Indeed, the dynamic component dominates the spread of precipitation change over ocean and continental coasts. The thermodynamic component explains most of the spread over inland regions, in particular over the Amazon forest.

This land-ocean contrast results from a different Clausius–Clapeyron scaling of surface specific humidity between land and ocean. Over ocean, relative humidity (RH) is nearly unchanged in the perturbed climate and so increases in water vapor closely follow the Clausius–Clapeyron relationship (O'Gorman and Muller 2010; Sherwood et al. 2010). However, over land, the Clausius–Clapeyron constitutes a weaker constraint. This is due to a strong decrease in surface RH that is directly influenced by moisture availability limitations on evaporation rates and by the amplification of surface warming over land compared to ocean (O'Gorman and Muller 2010; Byrne and O'Gorman 2013).

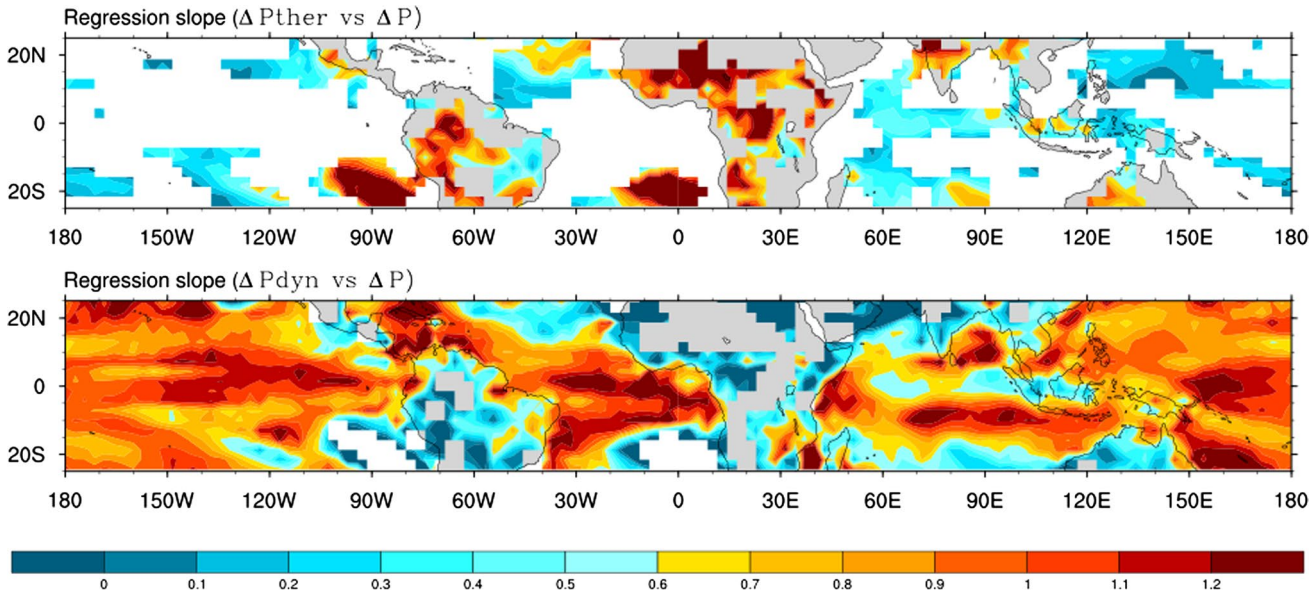

Fig. 2 Regression slopes of ΔP_{ther} versus ΔP (*upper panel*) and ΔP_{dyn} versus ΔP (*bottom panel*). Areas where the correlation of $(\Delta P_{ther}, \Delta P)$ and $(\Delta P_{dyn}, \Delta P)$ is not significant are *masked*. The slopes of the regression quantify the contribution of each component to the spread in precipitation projection change

3.2 Relative contributions of the fast response, hydrological sensitivity and climate sensitivity

In this section, we discuss the contributions of fast and long-term responses to precipitation uncertainties. The fast component characterizes the direct radiative forcing of GHG which modifies the radiative budget directly through fast atmospheric and surface changes independent of *global-mean* surface temperature changes. The slow component characterizes the feedbacks that are mediated by changes in global mean surface temperature.

The respective roles of carbon dioxide direct effect and climate warming in the spread of tropical precipitation responses are investigated by analysing the abrupt $4 \times CO_2$ simulations in which the atmospheric CO_2 concentration is abruptly quadrupled and then held fixed. The radiative forcing in the $4 \times CO_2$ simulation is equivalent to that produced in the RCP8.5 scenario at the end of the 21C. The patterns of precipitation as well as the inter-model spread being very similar between the two simulations (not shown), the abrupt $4 \times CO_2$ simulations can be used to assess the respective contributions of fast and long-term responses to the spread in precipitation change.

We express the dynamic and thermodynamic components (noted i in the equation) as follows:

$$\Delta P_i = \left(\frac{\partial P_i}{\partial CO_2}\right)_{Ts} \Delta CO_2 + \left(\frac{\partial P_i}{\partial Ts}\right)_{CO_2} \Delta Ts, \tag{4}$$

where $\left(\frac{\partial P_i}{\partial CO_2}\right)_{Ts} \Delta CO_2$ is the fast response and $\left(\frac{\partial P_i}{\partial Ts}\right)_{CO_2} \Delta Ts$ is the long-term response. ΔTs is the equilibrium global mean surface temperature change in response to CO_2 quadrupling. The fast component is computed from the first simulated year of abrupt $4 \times CO_2$. The long-term response is decomposed into two contributions: the local hydrological sensitivity $\left(\frac{\partial P_i}{\partial Ts}\right)_{CO_2}$ and the climate sensitivity ΔTs. The hydrological sensitivity is defined as the sensitivity of the precipitation rate to a change in temperature and is estimated through linear regression between ΔP_i and ΔTs from abrupt $4 \times CO_2$ simulations.

To assess the importance of each component in the spread of precipitation change, we compute the intermodel standard deviation of ΔP_i differently by varying only one term in each computation. We obtain 3 different computations of ΔP_i as follows:

$$\begin{aligned}
\Delta P_{i\,1} &= \left(\frac{\partial P_i}{\partial CO_2}\right)_{Ts} \Delta CO_2 + \left[\left[\left(\frac{\partial P_i}{\partial Ts}\right)_{CO_2} \Delta Ts\right]\right] \\
\Delta P_{i\,2} &= \left[\left[\left(\frac{\partial P_i}{\partial CO_2}\right)_{Ts} \Delta CO_2\right]\right] + \left(\frac{\partial P_i}{\partial Ts}\right)_{CO_2} [[\Delta Ts]] \\
\Delta P_{i\,3} &= \left[\left[\left(\frac{\partial P_i}{\partial CO_2}\right)_{Ts} \Delta CO_2\right]\right] + \left[\left[\left(\frac{\partial P_i}{\partial Ts}\right)_{CO_2}\right]\right] \Delta Ts,
\end{aligned} \tag{5}$$

where [[X]] denotes the multi-model mean of X. Computing the intermodel spread of $\Delta P_{i\,1}$, $\Delta P_{i\,2}$ and $\Delta P_{i\,3}$ allows

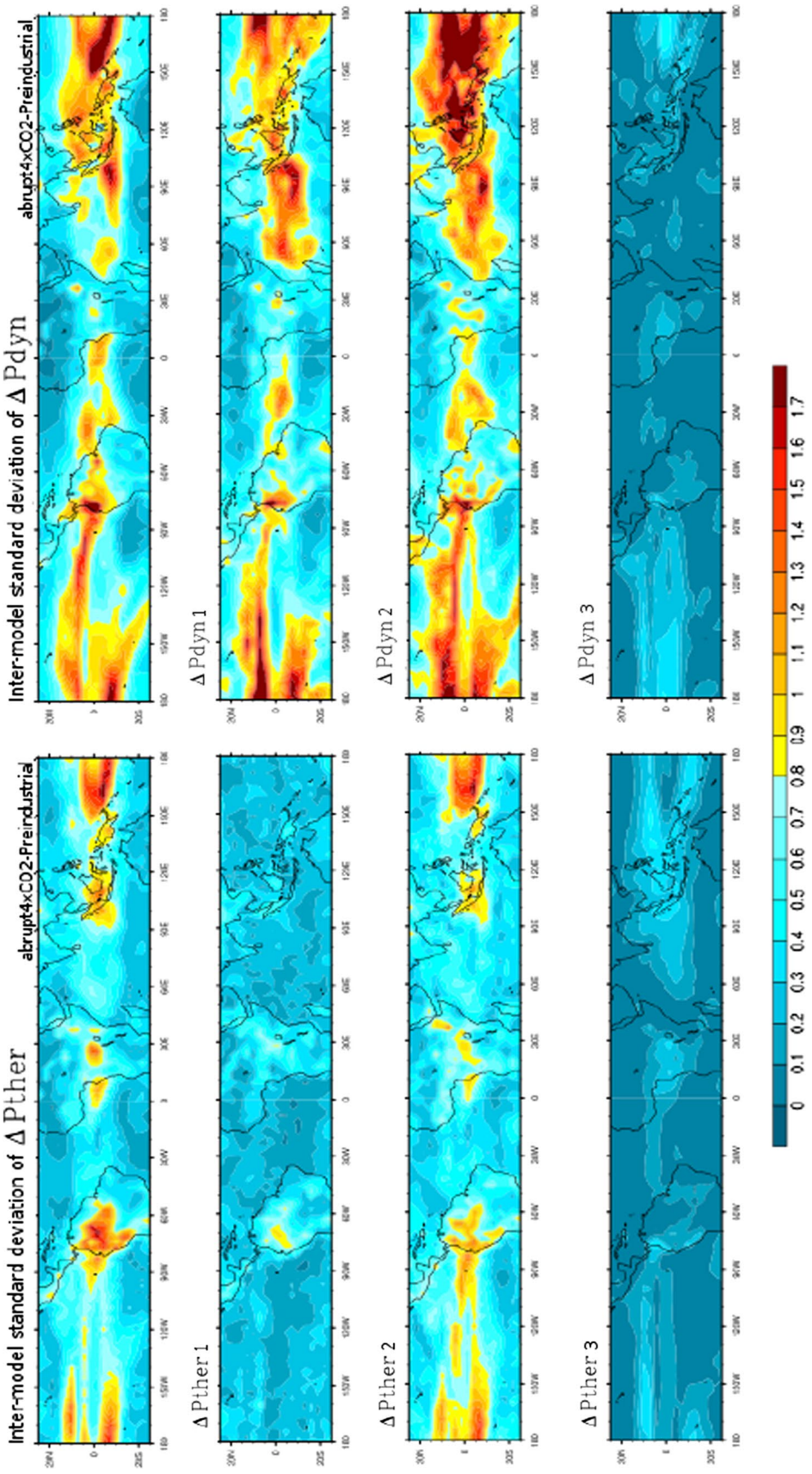

Fig. 3 Inter-model spread of the thermodynamic (*upper left panel*) and dynamic (*upper right panel*) components of precipitation changes computed from abrupt 4 × CO_2 simulations at the end of the 21C. The *three bottom panels* show the contributions of carbon dioxide direct effect ($\Delta P_{i\,1}$), hydrological sensitivity ($\Delta P_{i\,2}$) and climate sensitivity ($\Delta P_{i\,3}$) to the inter-model spread of the thermodynamic (*left*) and dynamic (*right*) components of precipitation changes. The methodology used is described in Sect. 3.2. Units: mm/day

us to isolate the contributions of the fast component, the hydrological sensitivity and the climate sensitivity to the total spread, respectively. These components are shown in Fig. 3. The residuals ($\Delta P_i - \sum_{j=1}^{3} \Delta P_{i\,j}$) are small (<0.1 mm/day).

For both thermodynamic and dynamic components, the precipitation uncertainty mediated by temperature change is dominated by uncertainties in the hydrological sensitivity (see Fig. 3, $\Delta P_{i\,2}$). The inter-model spread of climate sensitivity does not directly translate into the precipitation spread (see Fig. 3, $\Delta P_{i\,3}$). This result is consistent with Kent et al. (2015). The feedbacks associated with global warming affect the radiative budget and contribute to the hydrological sensitivity spread. These feedbacks include for instance the temperature feedback which induces an increase in LW emission due to higher temperatures affecting therefore the radiative budget.

In addition to these temperature-mediated feedbacks, the CO_2 radiative forcing contributes to the inter-model spread in precipitation change through its direct effect (see Fig. 3, $\Delta P_{dyn\,1}$). As defined in Boucher (2013) and Sherwood et al. (2015), the direct effect of CO_2 (or CO_2 adjustment) refers to the changes that occur directly due to the forcing, without mediation by the *global-mean* temperature change. By decreasing the net upwelling longwave radiation at the top of the atmosphere (TOA) more than it affects the radiation at the surface, enhanced CO_2 concentrations weaken the radiative cooling of the atmosphere. As the strength of the atmospheric circulation is constrained by the radiative cooling, the precipitation is reduced in convergence regions and increased in divergence regions.

In a coupled ocean-atmosphere-land system, the radiative effect of CO_2 and the fast circulation changes associated with it induce fast changes in surface temperature patterns, both over land and over ocean regions with relatively shallow mixed layers, which are part of the direct effect of CO_2 (Watanabe et al. 2012; Sherwood et al. 2015). The fast changes in SST patterns are, by construction, not captured by the fixed-SST $4 \times CO_2$ experiments. However they are captured by the climate system response to an abrupt $4 \times CO_2$ forcing, and contribute to the dynamical component of fast precipitation changes (see Fig. 3, $\Delta P_{dyn\,1}$). The fast changes in SST patterns can differ across models, and thus contribute to the spread in regional precipitation changes (Chadwick et al. 2014). However, the comparison of regional circulation and precipitation changes predicted by climate models in a hierarchy of experiments (first year of coupled ocean-atmosphere abrupt $4 \times CO_2$, atmosphere-only $4 \times CO_2$ with fixed SSTs, atmosphere-only with uniform SST warming, aquaplanet experiments) suggests that the effects of fast changes in SST patterns on regional responses are mostly confined over the equatorial oceans (Bony et al. 2013; He et al. 2014; He and Soden 2015) and that they increase the spread in these regions. Note that the slight global warming of the ocean (less than 1K) during the first year of abrupt $4 \times CO_2$ might also contribute to the spread of the regional precipitation response. However, this contribution is likely to be small since the spread of regional precipitation responses in simulations forced by a much larger global warming (a uniform +4K) is much smaller than the spread in the fast precipitation response during the first year of abrupt $4 \times CO_2$ simulations, although this argument does not account for the role of coupled processes that are only captured only by abrupt $4 \times CO_2$ simulations. However, we think that their impact is small, outside equatorial regions, as changes in atmospheric circulation are very similar between the first year of abrupt $4 \times CO_2$ and fixed-SST $4 \times CO_2$ simulations. Therefore, the spread of regional precipitation during the 1st year of abrupt $4 \times CO_2$ is primarily associated with the direct impact of the CO_2 forcing on the atmospheric circulation and on the fast changes in surface temperature patterns it induces over land and over ocean.

In contrast, the thermodynamic component is not much affected by the CO_2 radiative forcing, which leads to small changes and differences between models at the short time-scale (see Fig. 3, $\Delta P_{ther\,1}$). In fact, ΔP_{ther} is primarily explained by the increase of water vapor with warming through the Clausius–Clapeyron relationship (especially over ocean).

In conclusion, the inter-model spread in large-scale circulation results from differing direct effects of CO_2 on the large-scale circulation and from differing sensitivities of the vertical velocity to surface temperature changes. Over ocean, these two contributions reinforce each other. However, over land, they exert opposing effects on the circulation strength introducing an additional source of uncertainty on the sign of the total change (Bony et al. 2013). Over land, the spread in ΔP mostly results from the spread in the hydrological sensitivity of ΔP_{ther}.

4 Interpretation of the spread in the hydrological sensitivity

4.1 Role of surface evaporation in the spread of the thermodynamic component

The thermodynamic component is related to changes in surface evaporation, moisture advection and present-day vertical velocity $\overline{\omega}$ (see Eq. 3). In this section, we investigate the respective roles of these components in the inter-model spread of $\frac{dP_{ther}}{dTs}$. To do so we regress each of these components against $\frac{dP_{ther}}{dTs}$ following the same methodology as described in Sect. 3.1. Patterns are shown in Fig. 4. The slopes of the regression quantify the contribution of each component to the inter-model spread in $\frac{dP_{ther}}{dTs}$.

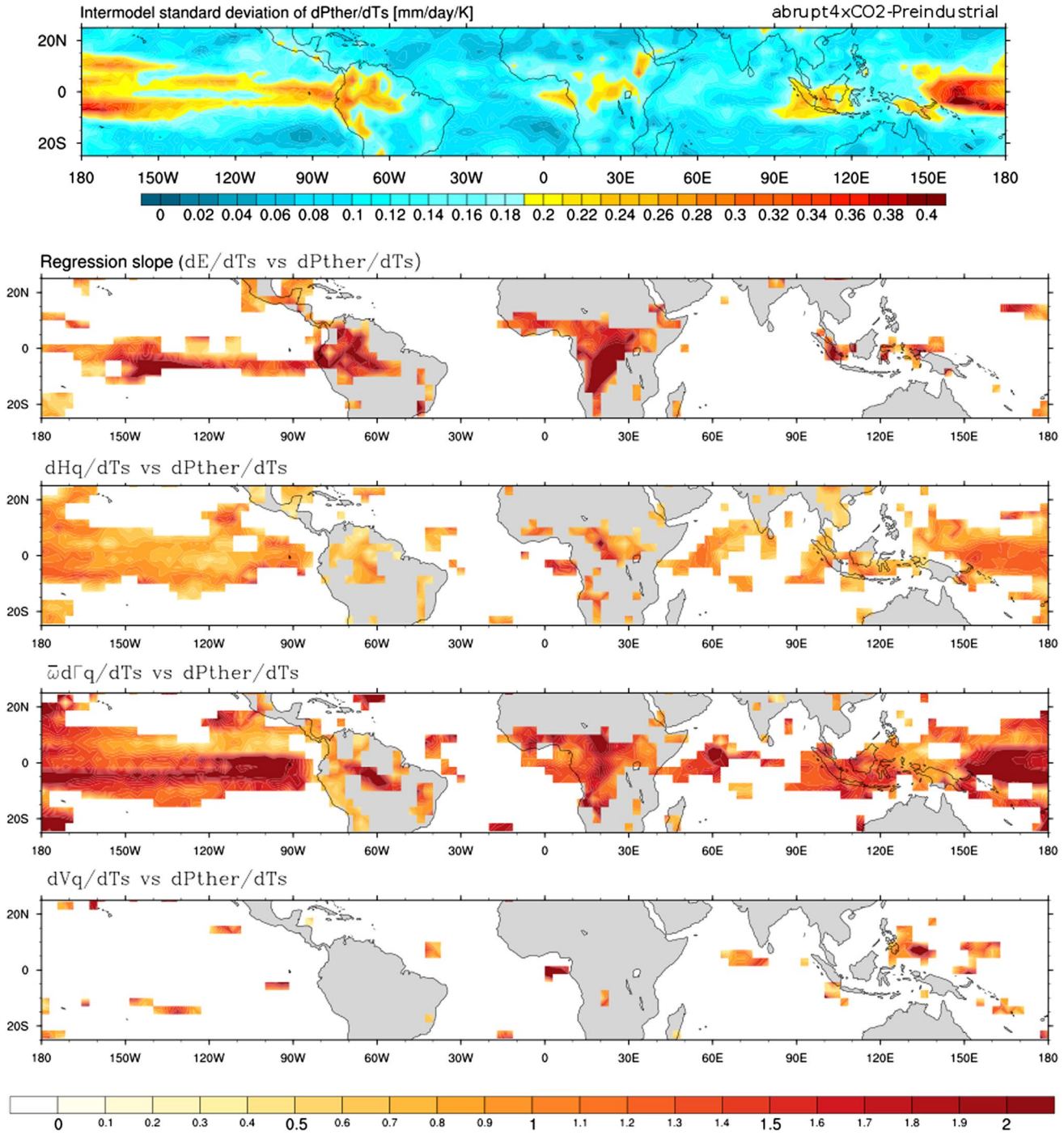

Fig. 4 Inter-model spread of the sensitivity of the thermodynamic component to sea surface temperature estimated through linear regression from abrupt 4 × CO_2 simulations (*upper panel*). The *four bottom panels* show the regression slopes of the *lines* giving the sensitivity of ΔP_{ther} components (defined by Eq. 3) to surface warming as a function of $\frac{dP_{ther}}{dTs}$. Areas where the correlation of $\frac{dP_{ther}}{dTs}$ and its components is not significant are *masked*. The slopes of the regression quantify the contribution of each component to the total spread

Two contributions are important for $\frac{dP_{ther}}{dTs}$ spread over land: surface evaporation ($\frac{dE}{dTs}$) and moisture vertical advection ($\frac{\overline{\omega} d\Gamma_q}{dTs}$), with a dominant contribution from evaporation. The spread of the vertical advection term is related to differing RH changes. This response is modulated by evaporation. In fact, an increase in surface evaporation amplifies the WeGW response but opposes the dry-get-drier response. As a result, the magnitude of evaporation modulates the thermodynamic component of precipitation change, and thus contributes to the inter-model spread

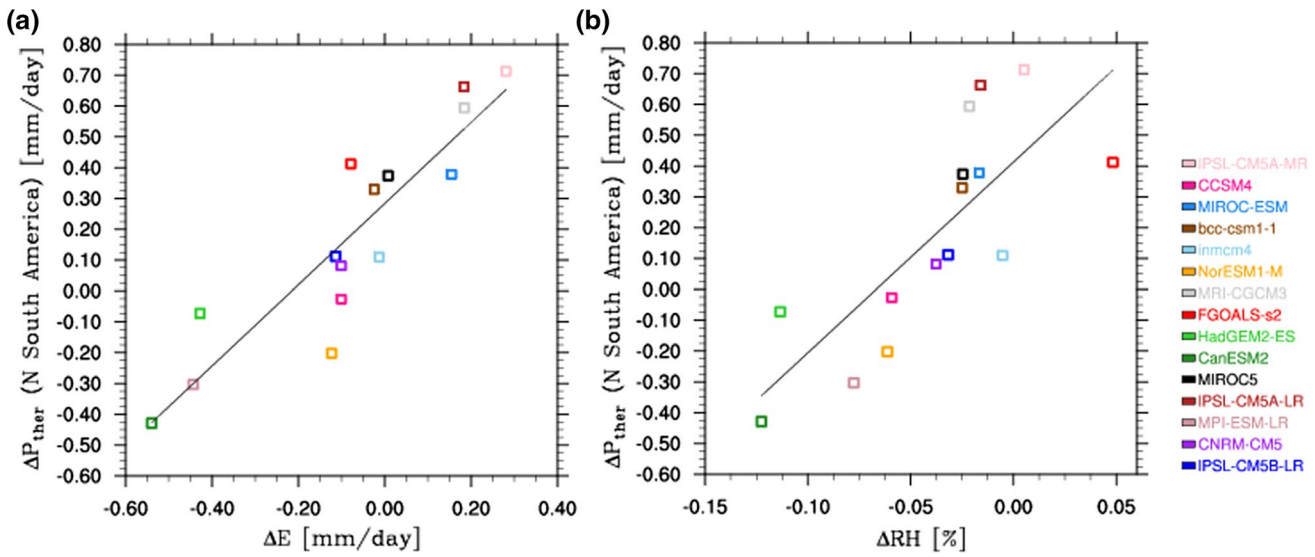

Fig. 5 Scatter plot of the thermodynamic component of precipitation change in RCP8.5 scenario versus **a** the change in surface evaporation (R = 0.9) and **b** the change in near-surface relative humidity (R = 0.76) over the northern part of South America (50–80W; 10S–10N)

over land. This is illustrated in Fig. 5a which clearly shows that models do not agree on the sign and magnitude of ΔP_{ther} and ΔE over South America. The strong correlation between ΔP_{ther} and evaporation change (inter-model correlation = 0.9) highlights the role played by the evaporation in inter-model differences in precipitation over land, and vice versa.

Lorenz et al. (2010) and Richter and Xie (2008) investigated the various mechanisms that contribute to surface evaporation change and identified the important role played by surface relative humidity over ocean: Decreased relative humidity leads to increased evaporation through its direct effect on the air-sea specific humidity difference and its indirect effect of relative humidity on cloudiness, and hence the net radiation at the surface. This anti-correlation between E and RH does not explain the inter-model spread in ΔP_{ther} over land. Indeed, Fig. 5b shows that ΔE and ΔRH are positively correlated, highlighting the close connection between ΔE and ΔRH. A decrease in RH results in a decrease in precipitation. As a result, less moisture is available over lakes and rivers, as well as, in the soil. These drier conditions over land reduce E. As surface evaporation is decreasing, moisture supply to the atmosphere decreases resulting in decreases in RH.

In addition to evaporation, the change in moisture vertical advection term ($\frac{\overline{\omega} d\Gamma_q}{dTs}$) due to the Clausius–Clapeyron relationship plays an important role in the inter-model spread of the thermodynamic component (see Fig. 4).

$\frac{\overline{\omega} d\Gamma_q}{dTs}$ depends on present-day vertical velocity $\overline{\omega}$ and vertical gradient of humidity $\frac{d\Gamma_q}{dTs}$. To quantify the respective roles of $\overline{\omega}$ and $\frac{d\Gamma_q}{dTs}$ in the inter-model spread, we compute the inter-model standard deviation differently assuming that either $\overline{\omega}$ or $\frac{d\Gamma_q}{dTs}$ is set to the multi-model mean (noted $[[X]]$), as described in Sect. 3.2. As shown in Fig. 6, over ocean and continental coasts, the inter-model spread of $\overline{\omega}\frac{d\Gamma_q}{dTs}$ is dominated by the spread in present-day climatology of the atmospheric circulation. Over inland regions, both changes in water vapor and present-day vertical velocity contribute to the precipitation spread. It implies that model biases and differences in the simulation of present-day circulation (and hence precipitation) lead to biases and differences in the projections of future precipitation change (Mitchell et al. 1987; Bony et al. 2013). Hopefully, this also indicates that this component of regional precipitation changes may be partly constrained by observations of the current climate.

$\frac{d\Gamma_q}{dTs}$ follows Clausius–Clapeyron scaling which can be directly evaluated assuming an unchanged distribution of relative humidity. This is a good approximation over ocean. However, there are deviations from Clausius–Clapeyron scaling of water vapor over land explained by decreases in surface relative humidity (O'Gorman and Muller 2010). Relative humidity contributes, therefore, to inter-model spread in precipitation through its impact on evaporation and moisture vertical advection. The role of relative humidity over land is emphasized by plotting ΔP_{ther} as a function of relative humidity changes (see Fig. 5b). We can see that ΔP_{ther} and ΔRH are highly correlated (correlation = 0.76) which highlights a close connection between ΔP_{ther}, ΔE and ΔRH.

Relative humidity is expected to decrease over most land areas as temperatures increase and in particular over South America (see Fig. 5b) (O'Gorman and Muller 2010; Fasullo 2012). This is directly linked to moisture availability

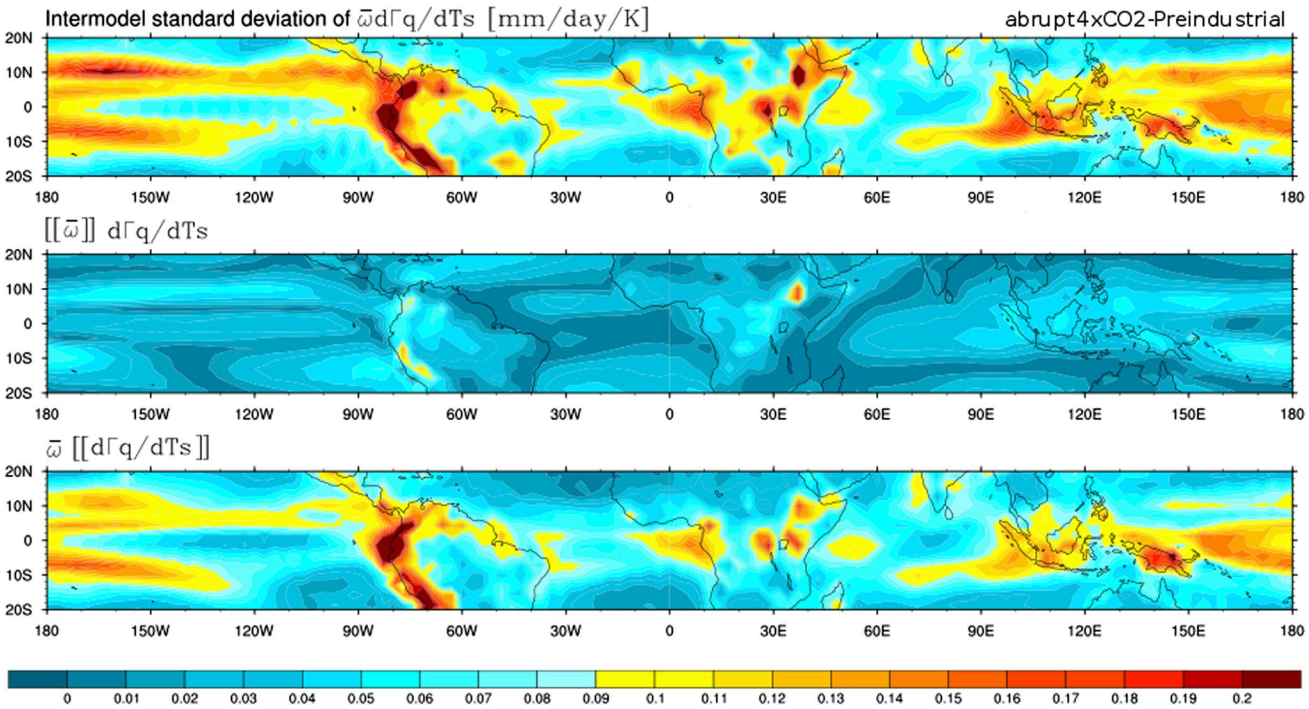

Fig. 6 Inter-model standard deviation of $\overline{\omega}\frac{d\Gamma_q}{dTs}$ (*upper panel*). The *two bottom panels* show respectively the contributions of the vertical advection of water vapor $[[\overline{\omega}]]\frac{d\Gamma_q}{dTs}$ and present-day vertical velocity $\overline{\omega}[[\frac{d\Gamma_q}{dTs}]]$ to the total spread. For these *two panels*, the inter-model standard deviation is computed differently by varying only one component of the advection term and setting the other one to the multi-model mean (noted [[X]])

limitations on evaporation rates over land. In addition, the land-ocean contrast in surface warming contributes to the decrease of relative humidity over land through the role of the ocean as a source of water vapor advected over land (O'Gorman and Muller 2010; Byrne and O'Gorman 2013). Indeed, air moving from ocean to land is governed by saturation temperatures of oceanic air. Over land, this air is warmed resulting in a decrease in its relative humidity because of limited air moistening over land (O'Gorman and Muller 2010; Byrne and O'Gorman 2013).

To summarize, the spread in ΔP_{ther} is dominated by ΔRH over land and by the spread in present-day climatology of $\overline{\omega}$ over ocean.

4.2 Role of cloud radiative effects in the spread of the dynamic component

In this section, we focus on the contributors to inter-model spread of the dynamic component ($\Gamma_q \Delta\overline{\omega}$) by focusing on the sensitivity of the vertical velocity to temperature change $\frac{d\overline{\omega}}{dTs}$. Following Chou et al. (2009) and Fermepin and Bony (2014), we use moist static energy diagnostics to examine the processes controlling the maintenance of regional precipitation change in the tropics.

Following the methodology proposed for the analysis of the water budget (see Sect. 2.2), the moist static energy budget ($h = C_pT + Lq + gz$) of the atmosphere can be expressed as:

$$F_s + Rad + \overline{\omega}\Gamma_h + H_h + V_h = 0 \tag{6}$$

where Fs is the sum of surface latent and sensible heat fluxes, Rad is the vertically-integrated radiative heating rate of the atmosphere, and Γ_h, V_h and H_h are defined similarly to Γ_q, V_q and H_q (see Sect. 2.2) using h instead of the specific humidity q.

$\overline{\omega}$ can be written as:

$$\overline{\omega} = \frac{-F_s}{\Gamma_h} + \frac{-Rad}{\Gamma_h} + \frac{-H_h}{\Gamma_h} + \frac{-V_h}{\Gamma_h} \tag{7}$$

The sensitivity of the vertical velocity to temperature change $\frac{d\overline{\omega}}{dTs}$ can be expressed as:

$$\frac{d\overline{\omega}}{dTs} = F_s' + Rad' + H_h' + \Gamma_h' + V_h' \tag{8}$$

with:

$$F_s' = -\frac{1}{\Gamma_h}\frac{dF_s}{dTs},$$

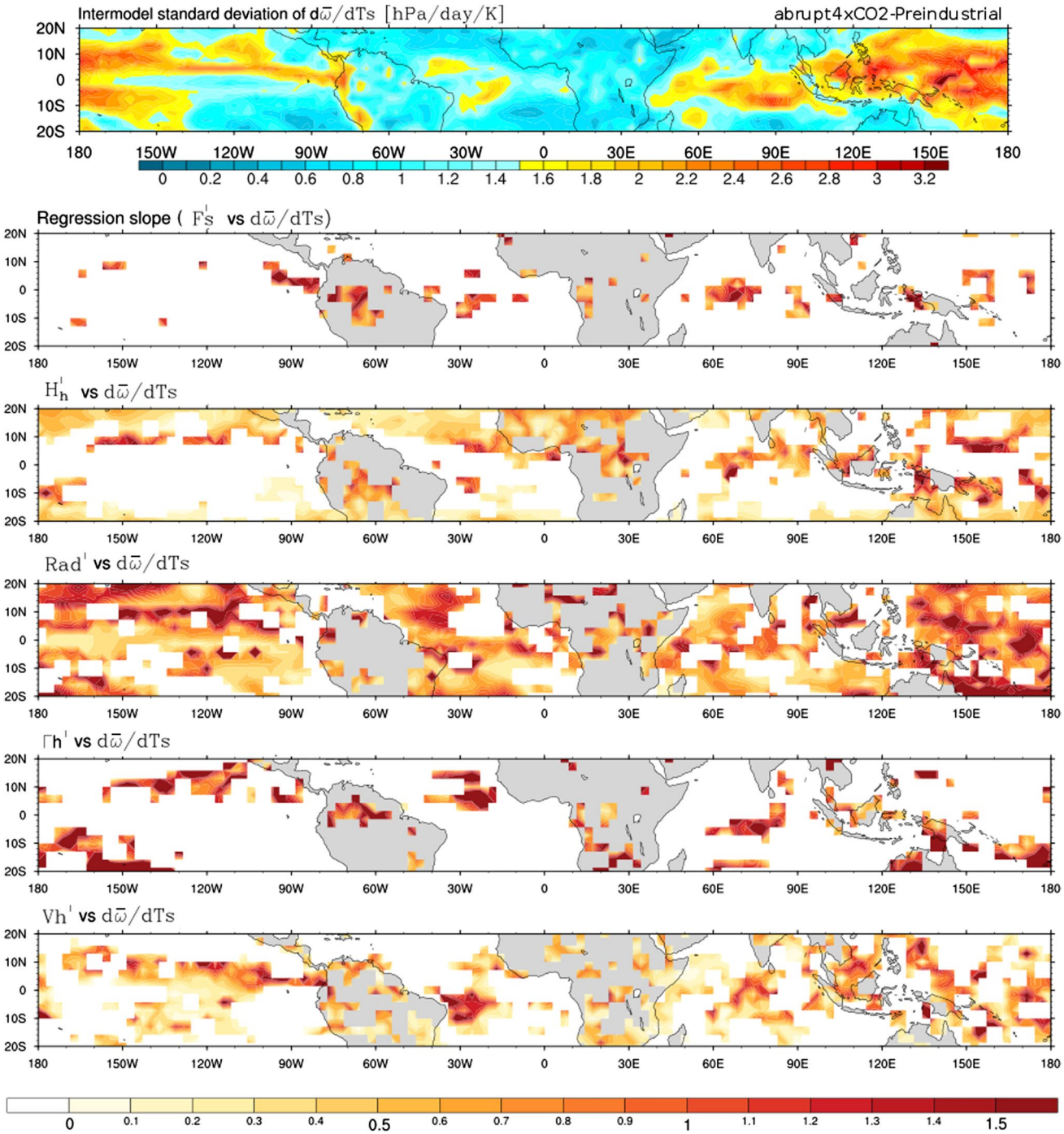

Fig. 7 Inter-model spread of the sensitivity of mean vertical velocity to sea surface temperature estimated through linear regression from abrupt 4 × CO_2 simulations (*upper panel*). The *five bottom panels* show the regression slopes of the lines giving the sensitivity of $\overline{\omega}$ components (defined by Eq. 8) to surface warming as a function of $\frac{d\overline{\omega}}{dTs}$. Areas where the correlation of $\frac{d\overline{\omega}}{dTs}$ and its components is not significant are *masked*. The slopes of the regression quantify the contribution of each component to the total spread

$$Rad' = -\frac{1}{\Gamma_h}\frac{dRad}{dTs},$$
$$H'_h = -\frac{1}{\Gamma_h}\frac{dH_h}{dTs},$$
$$\Gamma'_h = -\frac{\overline{\omega}}{\Gamma_h}\frac{d\Gamma_h}{dTs},$$
$$V'_h = -\frac{1}{\Gamma_h}\frac{dV_h}{dTs}.$$

We examine the relative roles of the different components by performing an inter-model regression of the dif-

ferent contributions versus $\frac{d\overline{\omega}}{dTs}$ following the same methodology as described in Sect. 3.1. Patterns are shown in Fig. 7. The slopes of the regression quantify the contribution of each component to the total spread of $\frac{d\overline{\omega}}{dTs}$.

Figure 7 shows that, over ocean, the rate of change of the atmospheric radiative heating with warming ($\frac{dRad}{dTs}$) is the dominant contributor to the regional large-scale circulation sensitivity to temperature and hence to the regional hydrological sensitivity. This result has been emphasized in different studies at the global scale (Mitchell et al. 1987; Stephens and Ellis 2008; Previdi 2010; O'Gorman et al. 2012; Voigt and Shaw 2015). In this work, we show that the inter-model spread in vertical velocity and hence in the dynamic component of regional precipitation changes is related to radiative heating. The strong relationship between ΔP_{dyn} and ΔRad (inter-model correlation = 0.65) is illustrated in Fig. 8 which also clearly show that models do not agree on the magnitude of ΔP_{dyn} and on both magnitude and sign of ΔRad over the Pacific Ocean.

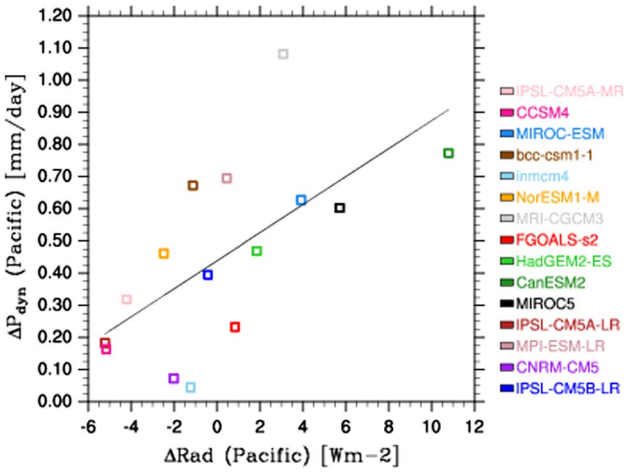

Fig. 8 Scatter plot of the dynamic component of precipitation change in RCP8.5 scenario versus the change in radiative heating (R = 0.65) in the tropical Pacific Ocean (15S–15N)

Several radiative feedbacks modulate the sensitivity of *Rad* to temperature. They are associated with changes in tropospheric temperature, water vapor and clouds. Previdi (2010) employed the radiative kernel technique to quantify these different components. Increased temperature enhances the radiative cooling of the troposphere through increased atmospheric longwave emission to space. Water vapor feedback tends to offset a significant portion of the increase in radiative cooling associated with temperature feedback and leads to a reduced rate of precipitation (Previdi 2010). Atmospheric Cloud radiative effects (ACRE) associated with deep convection act to weaken the radiative cooling of the atmosphere, while low-level clouds feedbacks act to increase it. Cloud radiative effects are not as large in magnitude as the temperature and water vapor feedbacks but they are the major source of inter-model spread in global hydrological sensitivity (Previdi 2010). Figure 9 shows that the dominant role of cloud radiative effects in the spread of *Rad* is also found at the regional scale: the inter-model differences in *Rad* are related to cloud changes, particularly by longwave cloud radiative effects which enhance the net diabatic heating of the atmospheric column and enhance large-scale circulation and precipitation.

In addition to ACRE, $\frac{dV_h}{dTs}$ which relates to how the shape of the vertical velocity profile varies with temperature, contributes to the spread of the dynamic component in many regions of the tropical oceans (see Fig. 9). This is illustrated in Fig. 10 which shows the normalized

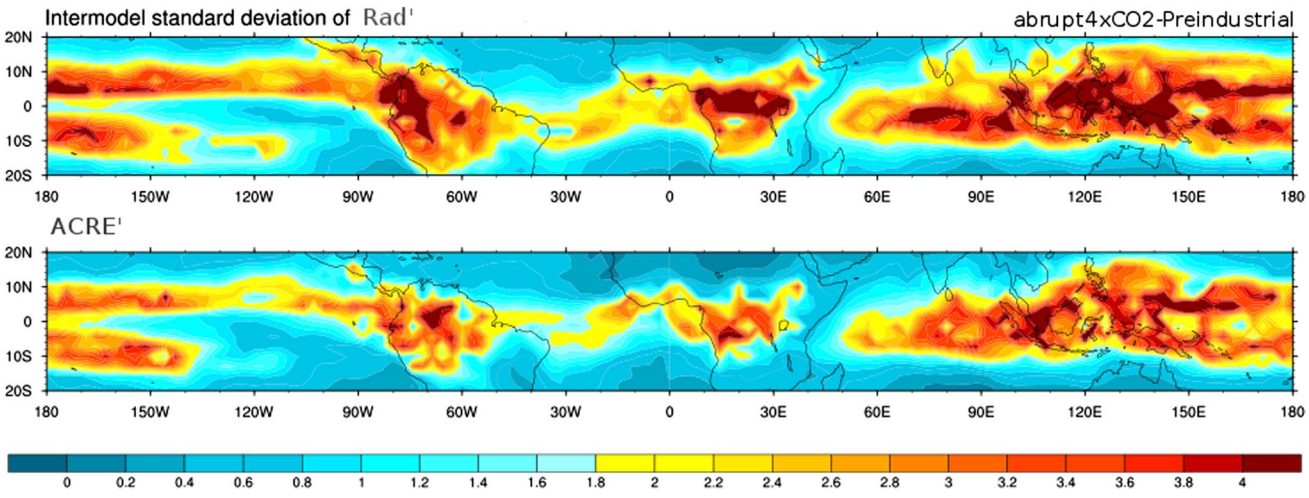

Fig. 9 inter-model standard deviations of the sensitivity of radiative heating (Rad') and Atmospheric cloud radiative effect ($ACRE' = \frac{1}{\Gamma_h}\frac{-dACRE}{dTs}$) to temperature computed from abrupt 4 × CO_2 simulations

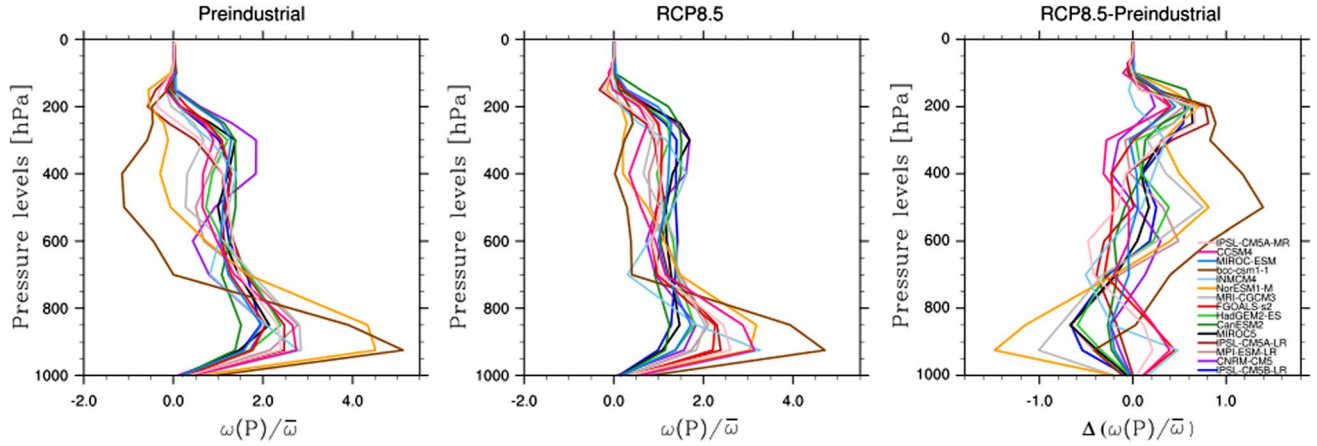

Fig. 10 Normalized vertical velocity profile $\frac{\omega(p)}{\overline{\omega}}$ over the Northern East Pacific (80–120W; 3–10N) for CMIP5 models computed from the preindustrial and RCP8.5 scenarios. The third panel represents the change in $\frac{\omega(p)}{\overline{\omega}}$

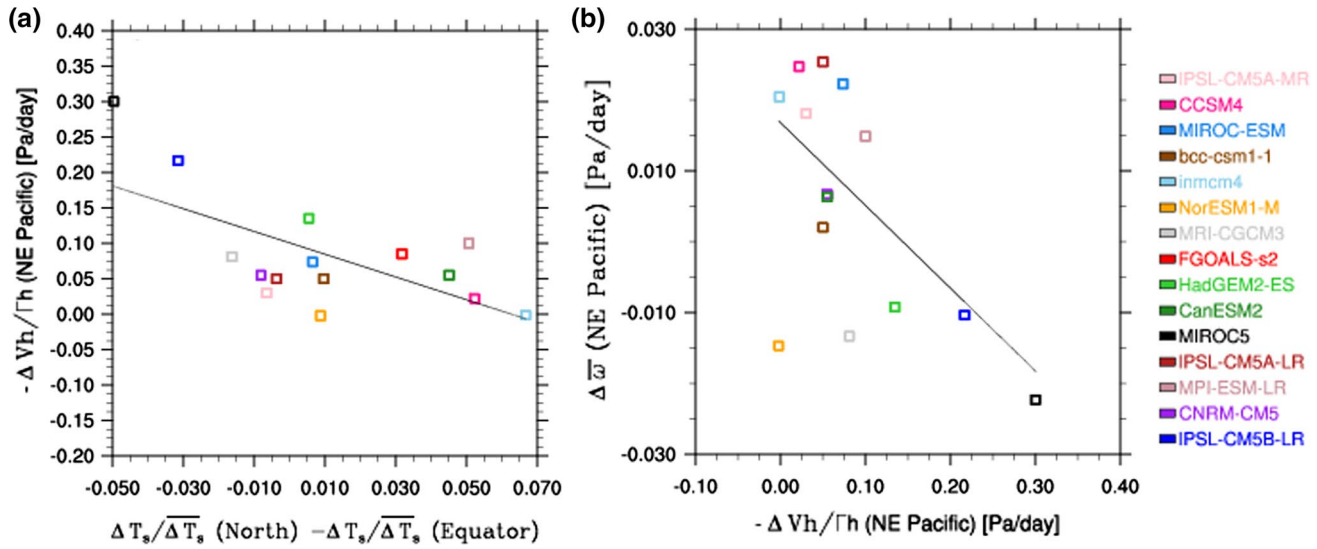

Fig. 11 **a** Scatter plot of $-\frac{1}{\Gamma_h}\Delta V_h$ in RCP8.5 scenario over the Northern East Pacific (80–120W; 5–15N) versus the change in meridional SST gradient computed as a difference between the normalized temperature in northern Pacific (80–120W; 5–15N) and at the equator (80–120W; 0–5N) (R = −0.62). **b** Scatter plot of $\Delta\overline{\omega}$ versus $-\frac{1}{\Gamma_h}\Delta V_h$ in RCP8.5 scenario over the Northern East Pacific (80–120W; 5–15N) (R = −0.5)

vertical velocity profile $\frac{\omega(p)}{\overline{\omega}}$ over the North equatorial Eastern Pacific (80–120W; 3–10N) for CMIP5 models computed from the preindustrial and RCP8.5 scenarios. The vertical velocity in this particular region is characterized by a convective bottom-heavy profile with convergence below 800 hPa, consistent with the profile highlighted over the eastern Pacific ITCZ by Back and Bretherthon (2006) using reanalyses data (ERA40, NCEP, NCEP2). It was suggested that the bottom-heaviness of the profile in the east-central Pacific is driven by low-level convergence forced by strong meridional SST gradients (Back and Bretherthon 2006). This dynamical control of convection was also proposed to explain the ITCZ location (Lindzen and Nigam 1987; Oueslati and Bellon 2013).

In response to global warming, CMIP5 models predict different changes in the shape of the vertical velocity profile. A common feature among all models is a deepening of convection and a less pronounced bottom-heavy profile. The theory of Back and Bretherthon (2006) would suggest that this is associated with a weaker meridional SST gradient in the RCP8.5 scenario, a hypothesis confirmed by RCP8.5 simulations (see Fig. 11a). Apart from this common characteristic, the response of the vertical velocity profile to global warming is very different across CMIP5

models (see Fig. 11b). As a result, the inter-model spread in the dynamic component of precipitation is related to not only from the intensity of ω but also from the shape of ω profile (see Fig. 11b), consistently with inter-model differences in meridional SST gradient (see Fig. 11a). The SST pattern influences precipitation thermodynamically through changes in convective instability but also dynamically through its gradient (Xie et al. 2010; Ma and Xie 2013), contributing therefore to inter-model spread in precipitation projections.

5 Conclusions

Precipitation projections from climate models remain quite uncertain at the regional scale. This study unravels and clarifies the primary contributors to the inter-model spread in these projections among CMIP5 climate models. Consistently with Kent et al. (2015), we show that the spread in regional precipitation projections is not related to the spread in climate sensitivity. As highlighted in previous studies (Lambert and Allen 2009; O'Gorman and Muller 2010; Muller and O'Gorman 2011), land and ocean show contrasted responses in precipitation change. In this study, we show that the contributors to the inter-model spread over land and ocean are also different:

- The spread in precipitation change is dominated by thermodynamical changes over inland regions, and by dynamical changes over ocean and continental coasts. This conclusion might seem inconsistent with Kent et al. (2015)'s suggestions that both over land and ocean, the intermodel uncertainty of regional precipitation change is predominantly related to spatial shifts in convection and convergence. However it is not. The apparent contradiction comes from the fact that the dynamical/thermodynamical components are defined differently in Kent et al. (2015) and in this study. In Kent et al. (2015), the dynamical component is only related to the shift of convective features (their term relative to the circulation weakening is combined with the thermodynamic component and surface relative humidity change, and so the weakening component is largely compensated by their thermodynamical component) while in our study, it accounts for all dynamical changes.
- Over land, the spread in ΔP primarily relates to the spread in surface evaporation which is explained by limited moisture availability over land and decreases in relative humidity near the surface (O'Gorman and Muller 2010; Byrne and O'Gorman 2013). The changes in relative humidity are related to land-ocean warming contrast (O'Gorman and Muller 2010; Byrne and O'Gorman 2013). A secondary contribution to the spread in ΔP over land results from present-day climatology of the atmospheric circulation.
- Over ocean, the spread in ΔP primarily relates to the spread in atmospheric cloud radiative effects and in the vertical structure of ω vertical profile. This latter is due to differing changes in the meridional SST gradient. Further investigation will be needed to assess the role of cloud radiative effects as a driver of precipitation uncertainties. This could be addressed by using COOKIE (Clouds On/Off Klimate Intercomparison Experiment) (Stevens et al. 2012) numerical experiments in which clouds are made transparent to radiation.

This study shows that two types of processes are associated with the uncertainty in regional precipitation response to enhanced greenhouse gases:

- the coupling between cloud radiative effects and circulation, and its dependence on SST gradients, whose understanding and representation in climate models is recognized as being a Grand Challenge of climate science (Bony et al. 2015).
- the coupling between surface evaporation and precipitation over land.
- Advancing the physical understanding of these couplings and improving their representation in climate models might be crucial to reduce uncertainty in regional precipitation projections.

Acknowledgments This work was supported by the ClimaConf (ANR-10-CEPL-003) and the Isotropic (ANR-12-BS06-001) ANR projects. We acknowledge the World Climate Research Programme's Working Group on Coupled Modelling, which is responsible for CMIP, and we thank the climate modeling groups (listed in Table 1 of this paper) for producing and making available their model output. We also thank the two anonymous reviewers for their helpful comments.

References

Allen MR, Ingram WJ (2002) Constraints on future changes in climate and the hydrologic cycle. Nature 419:224–232

Andrews T, Forster PM, Boucher O, Bellouin N, Jones A (2010) Precipitation, radiative forcing and global temperature change. Geophys Res Lett 37:14701

Back LE, Bretherthon CS (2006) Geographic variability in the export of moist static energy and vertical motion profiles in the tropical pacific. Geophys Res Lett 33:L17810

Bony S, Bellon G, Klocke D, Sherwood S, Fermepin S, Denvil S (2013) Robust direct effect of carbon dioxide on tropical circulation and regional precipitation. Nat Geosci 6:447–451

Bony S, Stevens B, Frierson DMW, J C, Kageyama M, Pincus R, Shepherd TG, Sherwood SC, Siebesma AP, Sobel AH, Watanabe M, Webb MJ (2015) Clouds, circulation and climate sensitivity. Nat Geosci 8:261–268

Boucher O et al (2013) Climate change 2013: the physical science basis. In: Stocker TF et al (eds) Clouds and aerosols. Cambridge University Press, Cambridge, pp 571–657

Byrne MP, O'Gorman PA (2013) Link between land-ocean warming contrast and surface relative humidities in simulations whith coupled climate models. Geophys Res Lett 40:5223–5227

Chadwick R, Boutle I, Martin G (2013) Spatial patterns of precipitation change in CMIP5: why the rich dont get richer in the tropics. J Clim 26:3803–3822

Chadwick R, Good P, Andrews T, Martin G (2014) Surface warming patterns drive tropical rainfall pattern responses to CO_2 forcing on all timescales. Geophys Res Lett 41:610–615

Chou C, Neelin JD, Chen CA, Tu JY (2009) Evaluating the rich-get-richer mechanism in tropical precipitation change under global warming. J Clim 22:1982–2005

Fasullo J (2012) A mechanism for land-ocean contrasts in global monsoon trends in a warming climate. Clim Dyn 39:1137–1147

Fermepin S, Bony S (2014) Influence of low-cloud radiative effects on tropical circulation and precipitation. J Adv Model Earth Syst 6:513–526

Greve P, Orlowsky B, Mueller B, Sheffield J, Reichstein M, Seneviratne SI (2014) Global assessment of trends in wetting and drying over land. Nat Geosci 7:716–721

He J, Soden BJ (2015) Anthropogenic weakening of the tropical circulation: the relative roles of direct CO_2 forcing and sea surface temperature change. J Clim press 28:8728–8742

He J, Soden BJ, Kirtman B (2014) The robustness of the atmospheric circulation and precipitation response to future anthropogenic surface warming. Geophys Res Lett 41:2614–2622

Held IM, Soden BJ (2006) Robust responses of the hydrological cycle to global warming. J Clim 19:5686–5699

Huang P, Xie SP, Huang G, Huang R (2013) Patterns of the seasonal response of tropical rainfall to global warming. Nat Geosci 6:357–361

Kent C, Chadwick R, Rowell DP (2015) Understanding uncertainties in future projections of regional precipitation. J Clim 28:4390–4413

Knutson T, Manabe S (1995) Time-mean response over the tropical pacific to increased CO_2 in a coupled ocean-atmosphere model. J Clim 8:2181–2199

Lambert FH, Allen MR (2009) Are changes in global precipitation constrained by the tropospheric energy budget. J Clim 22:499–517

Lindzen RS, Nigam S (1987) On the role of the sea surface temperature gradients in forcing the low-level winds and convergence in the tropics. J Atmos Sci 44:2418–2436

Liu Z, Vavrus S, He F, Wen N, Zhong Y (2005) Rethinking tropical ocean response to global warming: the enhanced equatorial warming. J Clim 18:4684–4700

Lorenz DJ, DeWeaver ET, Vimont DJ (2010) Evaporation change and global warming: the role of net radiation and relative humidity. J Geophys Res 115:D20118

Ma J, Xie SP (2013) Regional patterns of sea surface temperature change: a source of uncertainty in future projections of precipitation and atmospheric circulation. J Clim 26:2482–2501

Mitchell JFB, Wilson CA, Cunnington W (1987) On CO_2 climate sensitivity and model dependence of results. Q J R Meteorol Soc 113:293–322

Muller CJ, O'Gorman PA (2011) An energetic perspective on the regional response of precipitation to climate change. Nat Clim Change 1:266–271

O'Gorman PA, Muller CJ (2010) How closely do changes in surface and column water vapor follow ClausiusClapeyron scaling in climate change simulations? Environ Res Lett 5:025207

O'Gorman PA, Allan RP, Byrne MP, Previdi M (2012) Energetic constraints on precipitation under climate change. Surv Geophys 33:585–608

Oueslati B, Bellon G (2013) Tropical precipitation regimes and mechanisms of regime transitions: contrasting two aquaplanet general circulation models. Clim Dyn 40:2345–2358

Previdi M (2010) Radiative feedbacks on global precipitation. Environ Res Lett 5:025211

Richter I, Xie SP (2008) Muted precipitation increase in global warming simulations: a surface evaporation perspective. J Geophys Res 113:D24118

Sherwood SC, Ingram W, Tsushima Y, Satoh M, Roberts M, Vidale PL, O'Gorman PA (2010) Relative humidity changes in a warmer climate. J Geophys Res 115:D09104

Sherwood SC, Bony S, Boucher O, Bretherton C, Forster PM, Gregory JM, Stevens B (2015) Adjustments in the forcing-feedback framework for understanding climate change. Bull Am Meteorol Soc 96:217–228

Stephens G, Ellis TD (2008) Controls of global-mean precipitation increases in global warming GCM experiments. J Clim 21:6141–6155

Stevens B, Bony S (2013) What are climate models missing? Science 340:1053–1054

Stevens B, Bony S, Webb M (2012) Clouds on-off klimate intercomparison experiment (COOKIE). http://www.euclipse.eu/wp4/wp4.html

Taylor KE, Stouffer RJ, Meehl GAA (2012) A summary of the CMIP5 experiment design. Bull Am Meteorol Soc 93:485–498

Voigt A, Shaw TA (2015) Circulation response to warming shaped by radiative changes of clouds and water vapor. Nat Geosci 8:102–106

Watanabe M, Shiogama H, Yoshimori M, Ogura T, Yokohata T, Okamoto H, Emori S, Kimoto M (2012) Fast and slow timescales in the tropical low-cloud response to increasing CO_2 in two climate models. Clim Dyn 39:1627–1641

Xie SP, Deser C, Vecchi GA, Ma J, Teng H, Wittenberg AT (2010) Global warming pattern formation: sea surface temperature and rainfall. J Clim 23:966–986